Electronic Supplementary Info

Mono-, di- and tetrarhenium Fischer carbene complexes with thienothiophene substituents

Zandria Lamprecht,[a] Shankara Radhakrishnan,[a] Alexander Hildebrandt,[b] Heinrich Lang,[b] David C. Liles,[a] Nora-ann Weststrate,[a,] and Simon Lotz[a] and Daniela I. Bezuidenhout,[a,c*]

[a.] *Department of Chemistry, University of Pretoria, Private Bag X20, Hatfield 0028, Pretoria, South Africa.*

[b.] *Technische Universität Chemnitz, Fakultät für Naturwissenschaften, Institut für Chemie, Anorganische Chemie, D-09107 Chemnitz, Germany.*

[c.] *Molecular Sciences Institute, School of Chemistry, University of the Witwatersrand, Johannesburg 2050, South Africa.*

Contents:

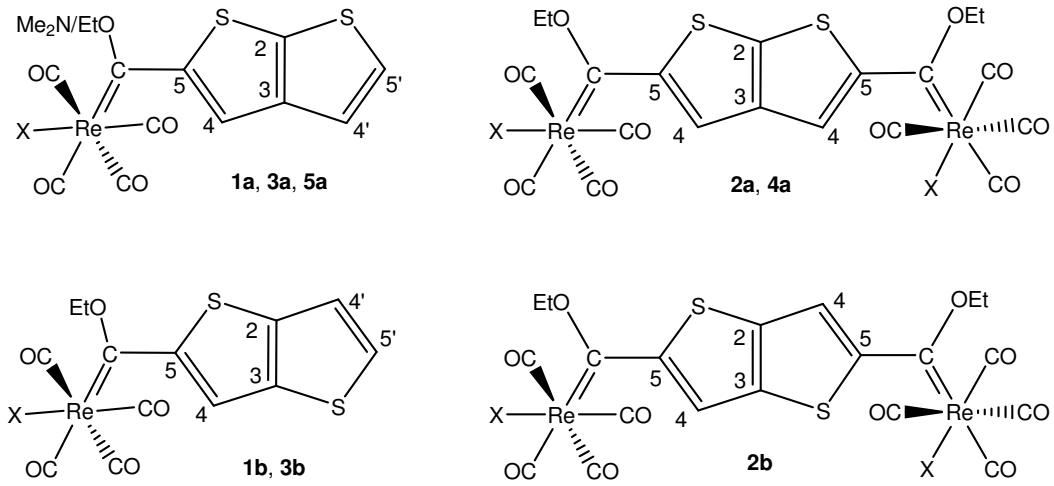

Figure S1: Atom numbering scheme used in NMR spectral assignment.

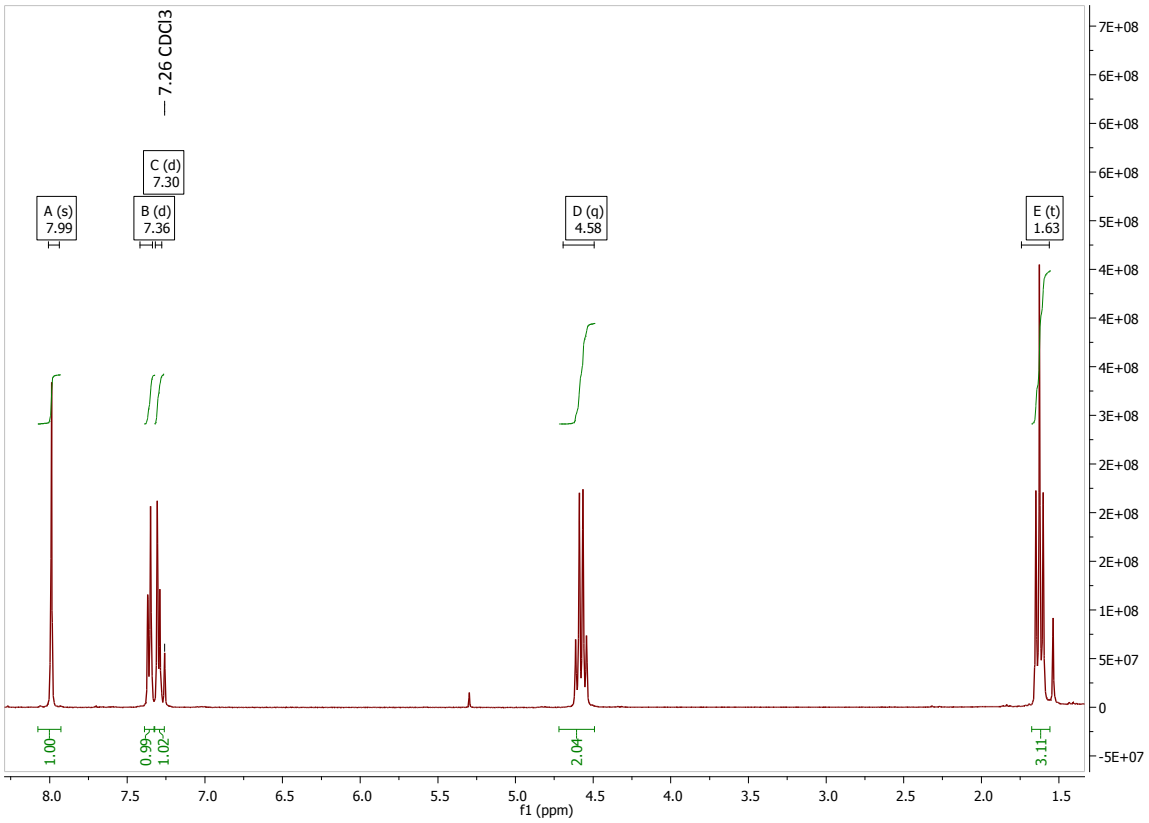

Figure S2: ^{1}H NMR spectrum of **1a** in $CDCl_3$.

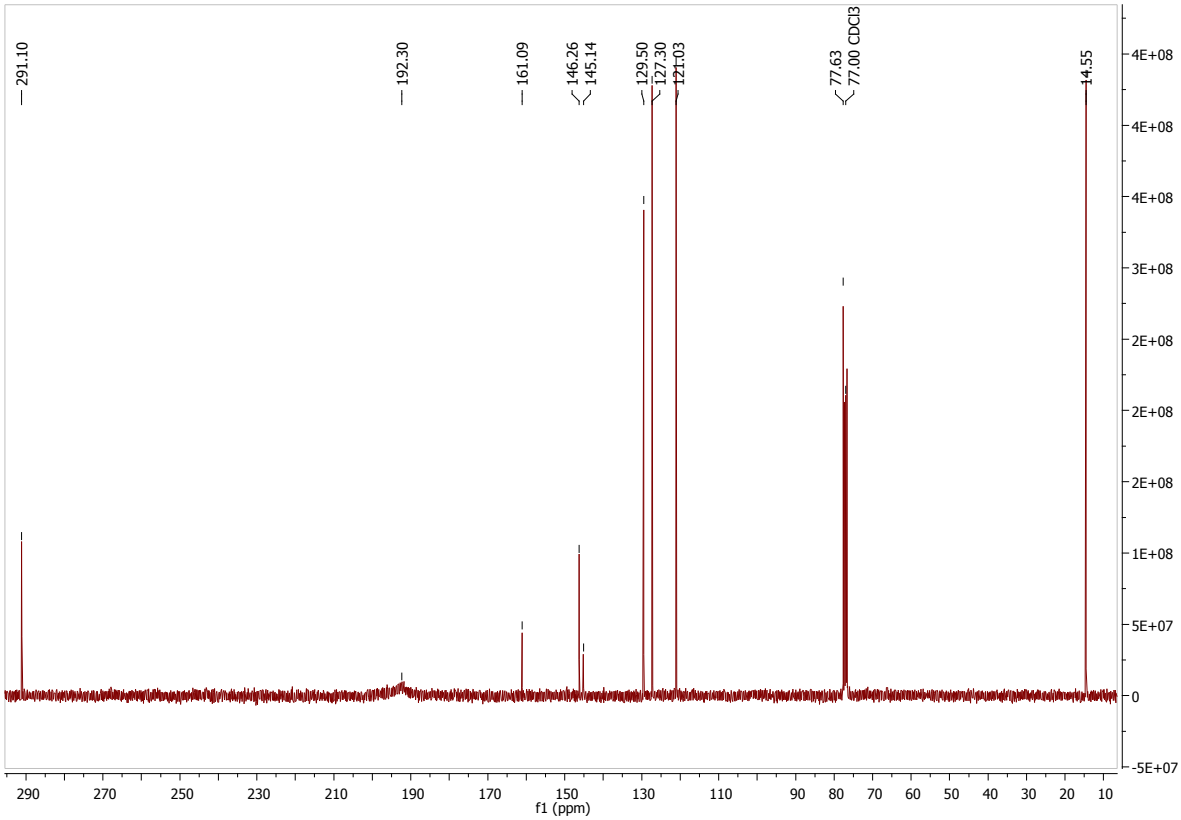

Figure S3: ^{13}C NMR spectrum of **1a** in $CDCl_3$.

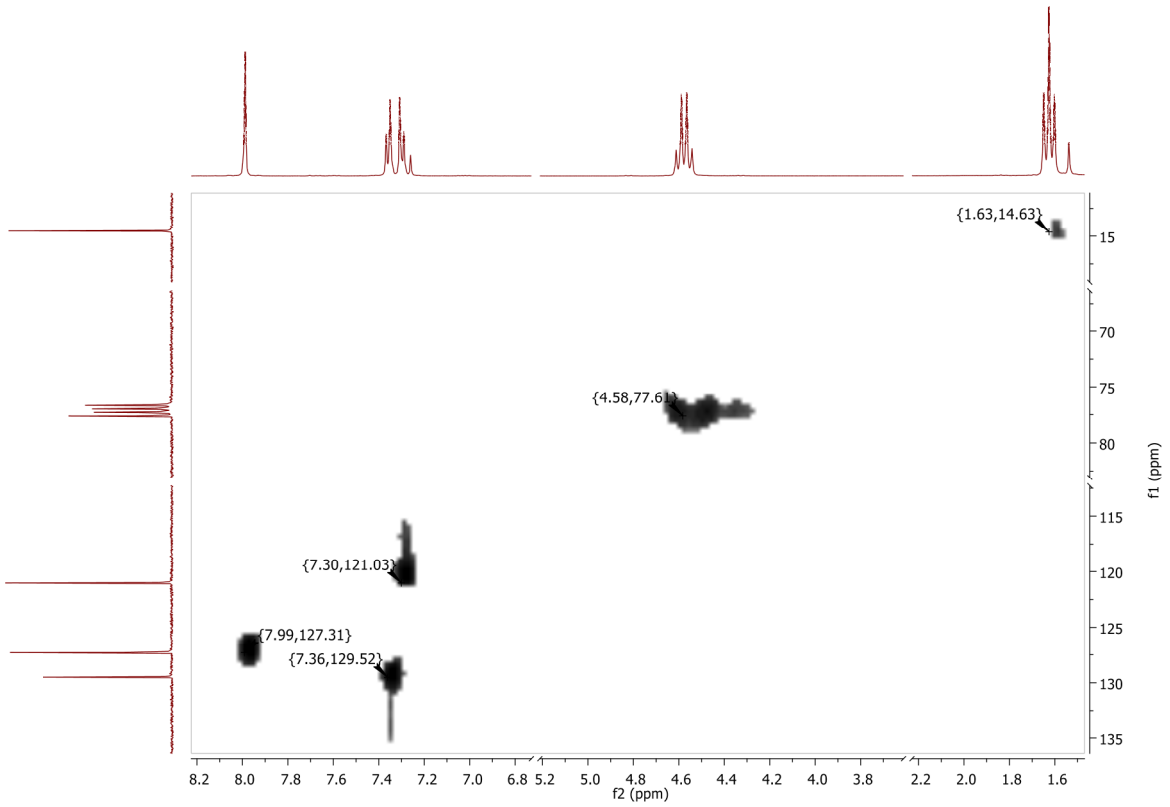

Figure S4: 2D [^{1}H, ^{13}C] HSQC NMR spectrum of **1a** in $CDCl_3$.

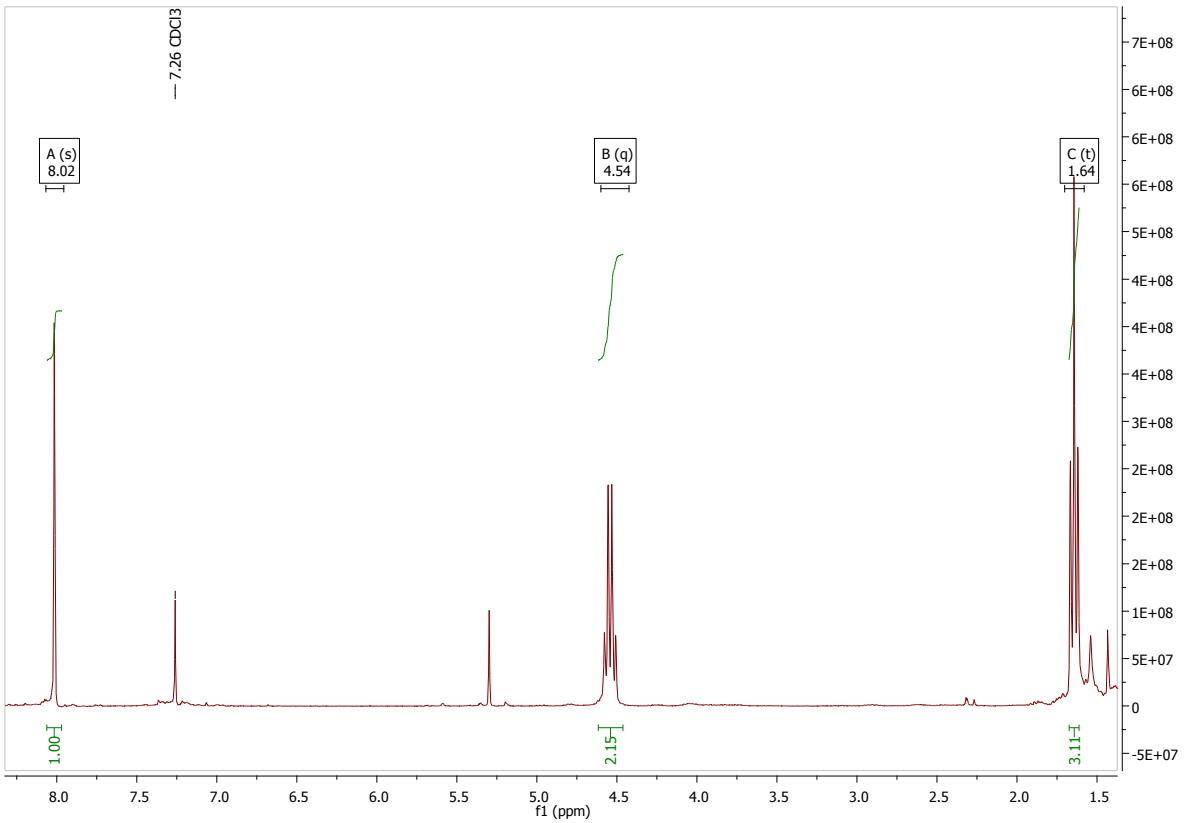

Figure S5: ^{1}H NMR spectrum of **2a** in $CDCl_3$.

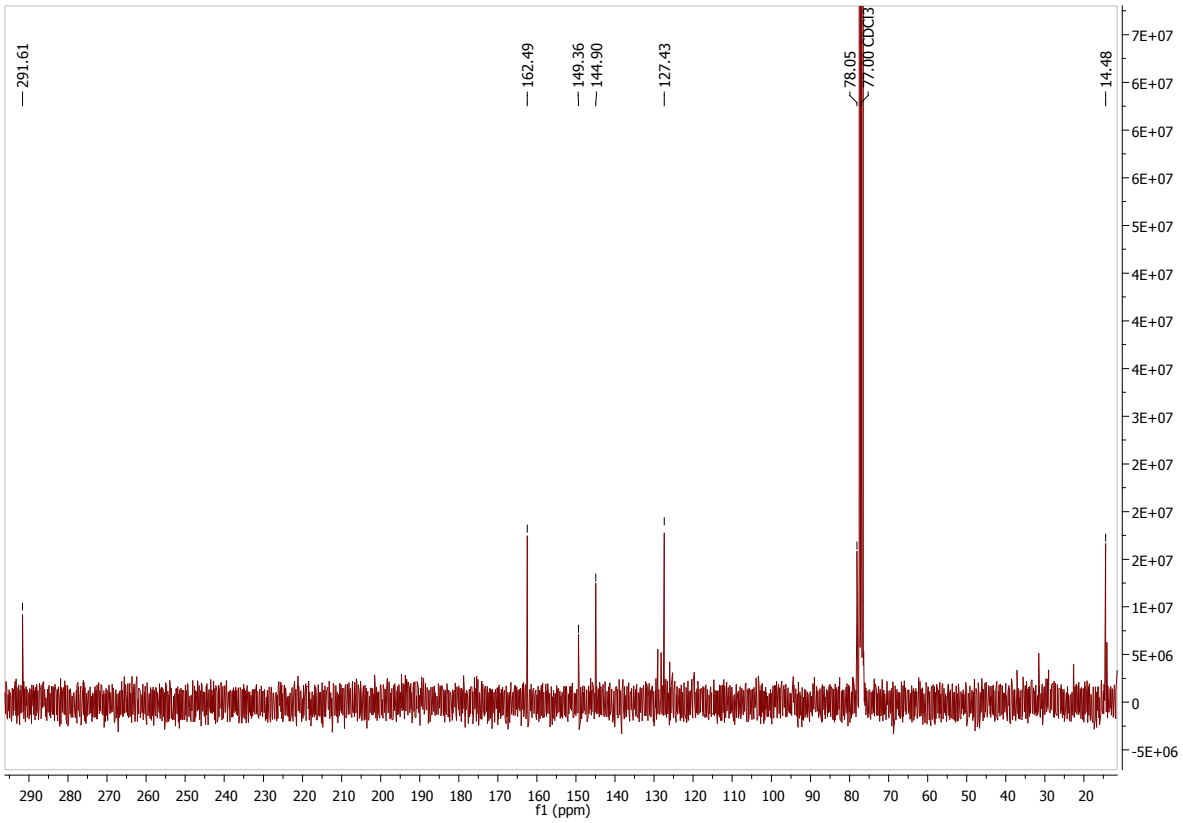

Figure S6: ^{13}C NMR spectrum of **2a** in $CDCl_3$.

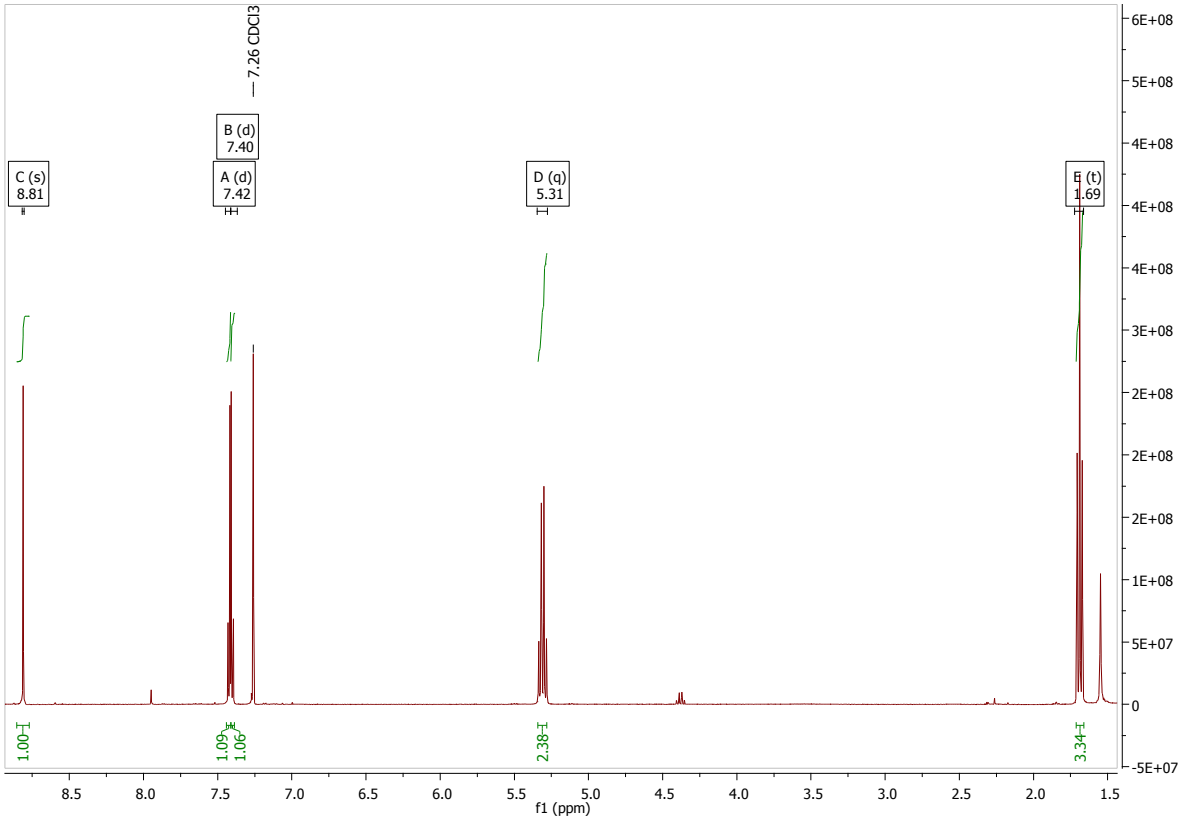

Figure S7: ^{1}H NMR spectrum of **3a** in $CDCl_3$.

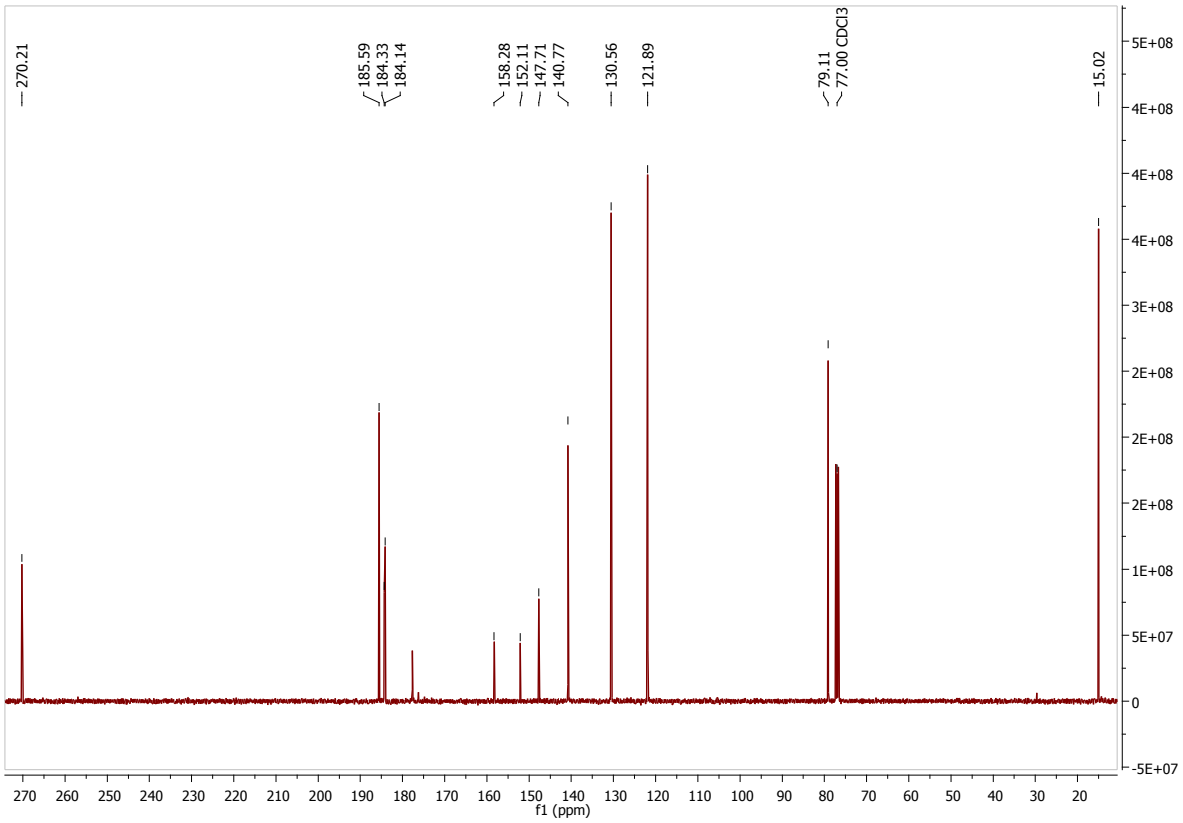

Figure S8: ^{13}C NMR spectrum of **3a** in $CDCl_3$.

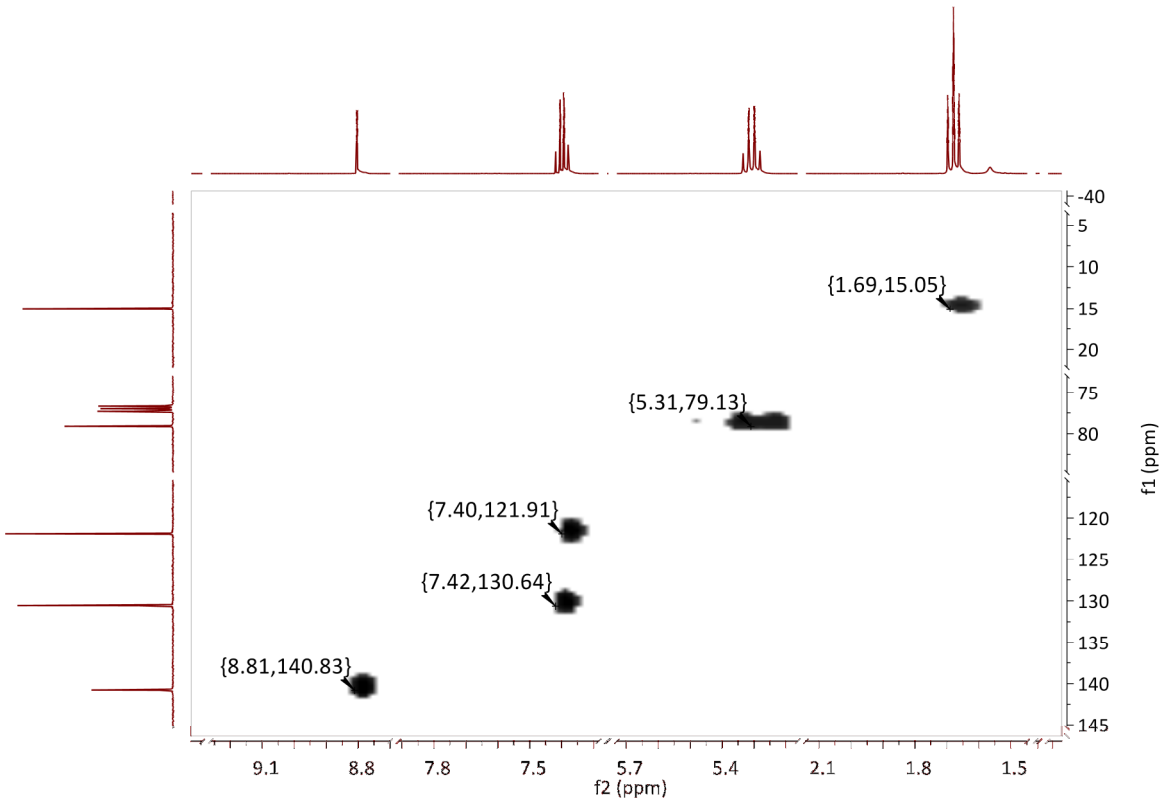

Figure S9: 2D [^{1}H, ^{13}C] HSQC NMR spectrum of **3a** in $CDCl_3$.

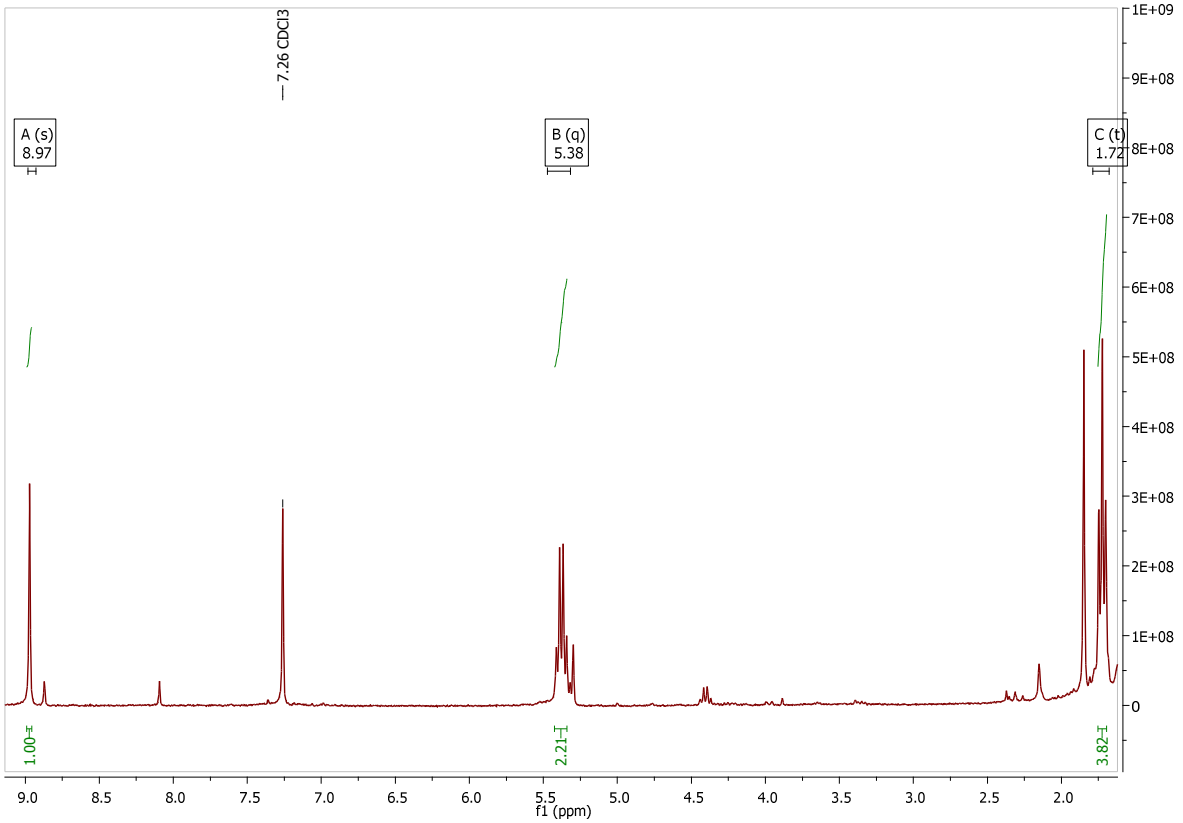

Figure S10: ^{1}H NMR spectrum of **4a** in $CDCl_3$.

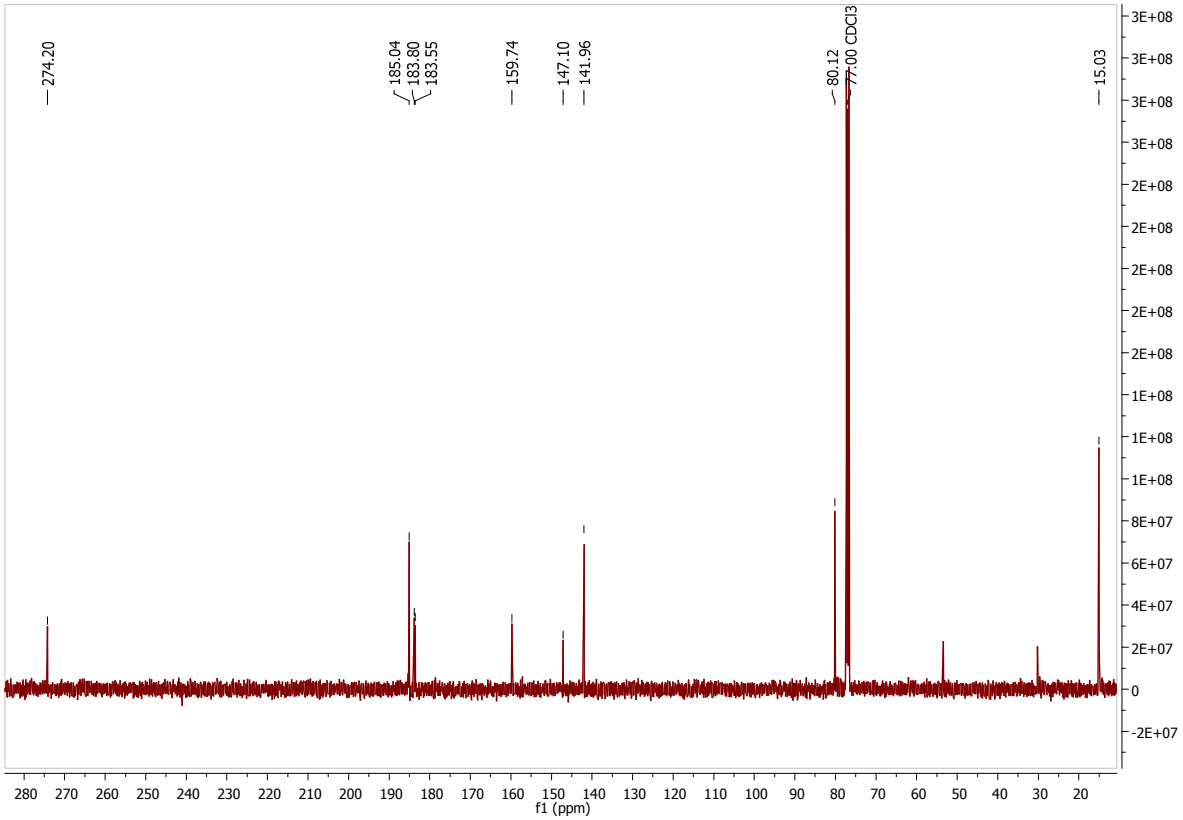

Figure S11: ^{13}C NMR spectrum of **4a** in $CDCl_3$.

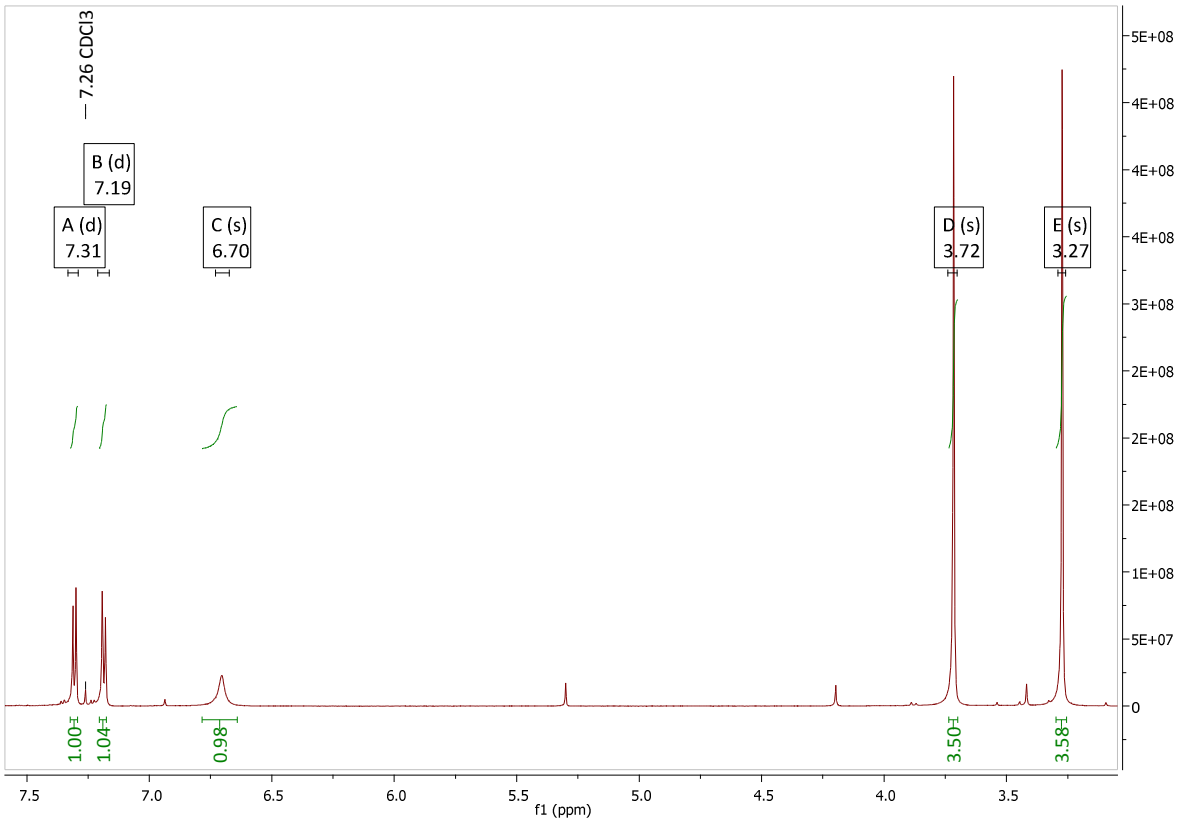

Figure S12: ^{1}H NMR spectrum of **5a** in $CDCl_3$.

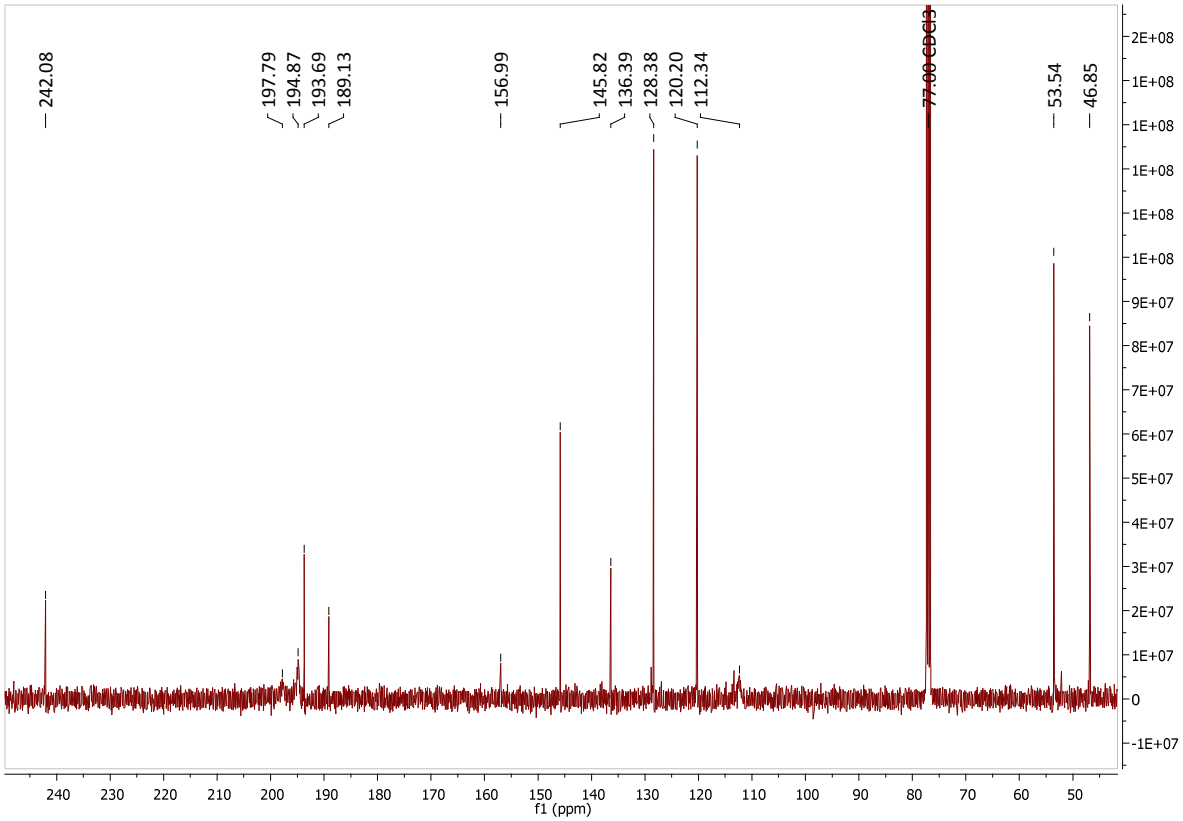

Figure S13: ^{13}C NMR spectrum of **5a** in $CDCl_3$.

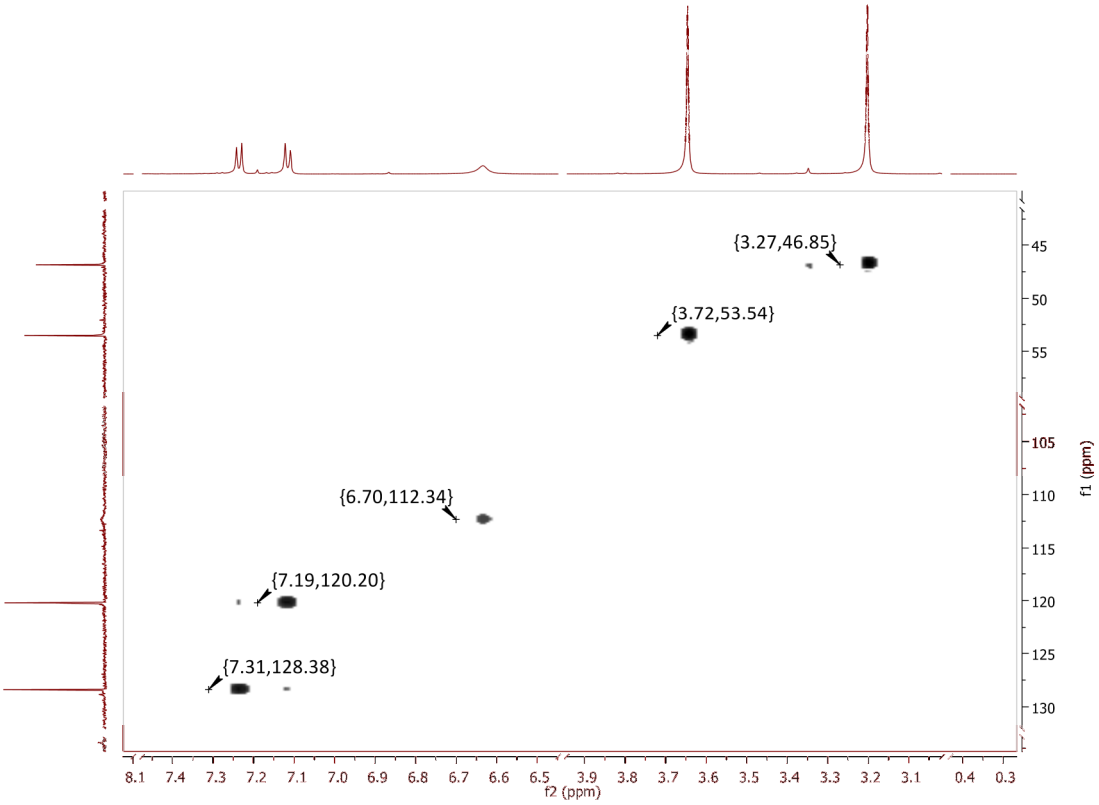

Figure S14: 2D [^{1}H, ^{13}C] HSQC NMR spectrum of **5a** in $CDCl_3$.

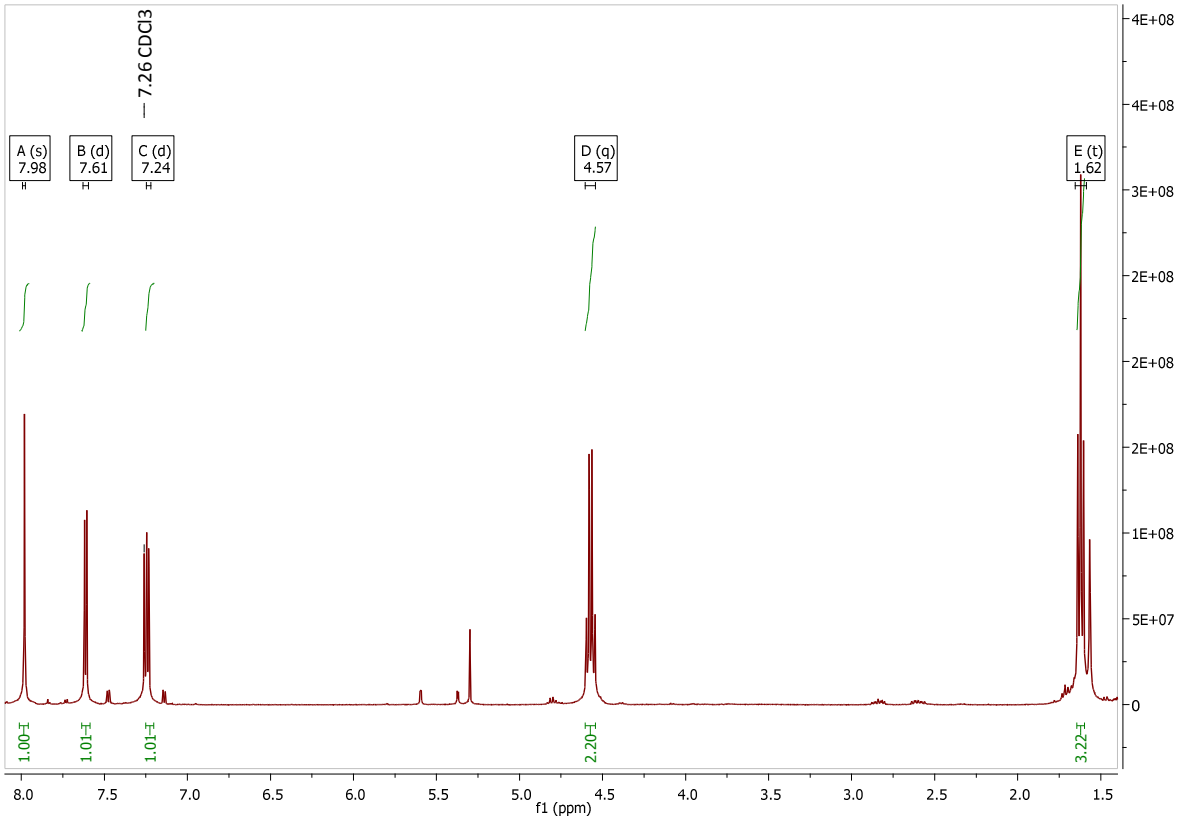

Figure S15: ^{1}H NMR spectrum of **1b** in $CDCl_3$.

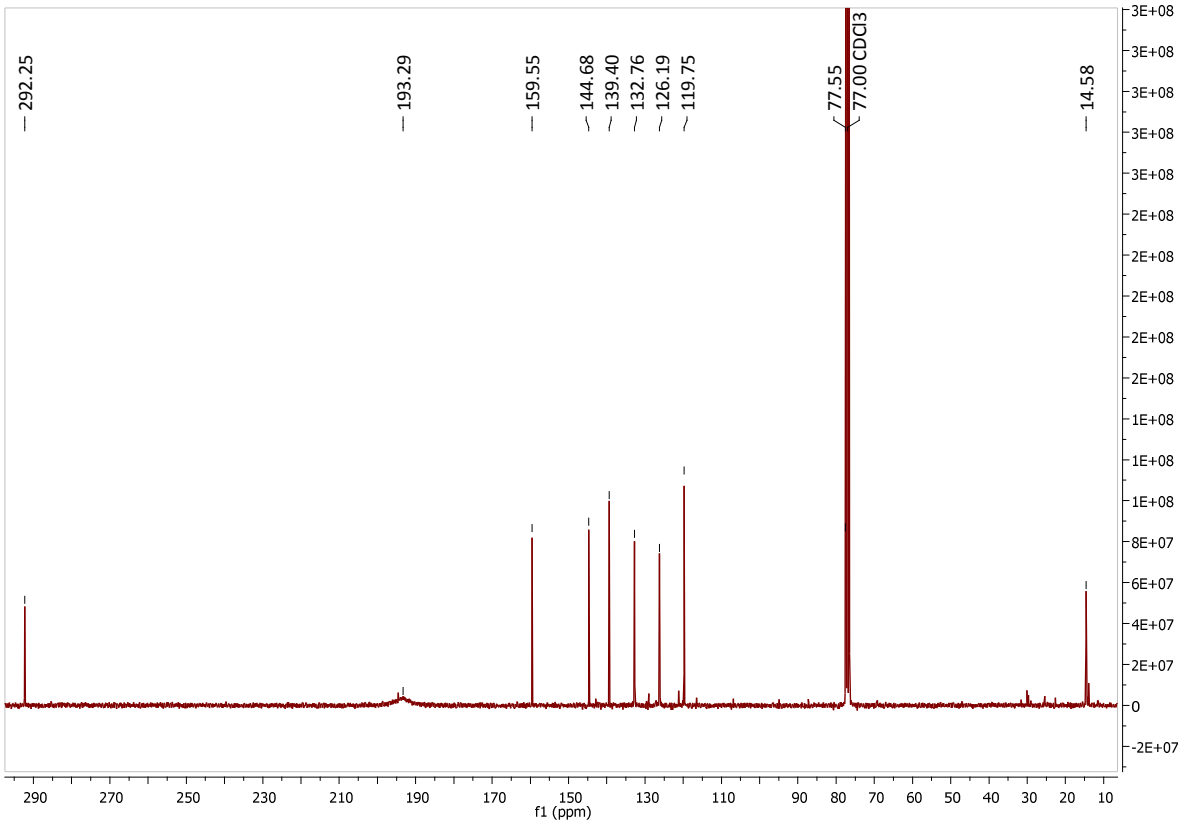

Figure S16: ^{13}C NMR spectrum of **1b** in $CDCl_3$.

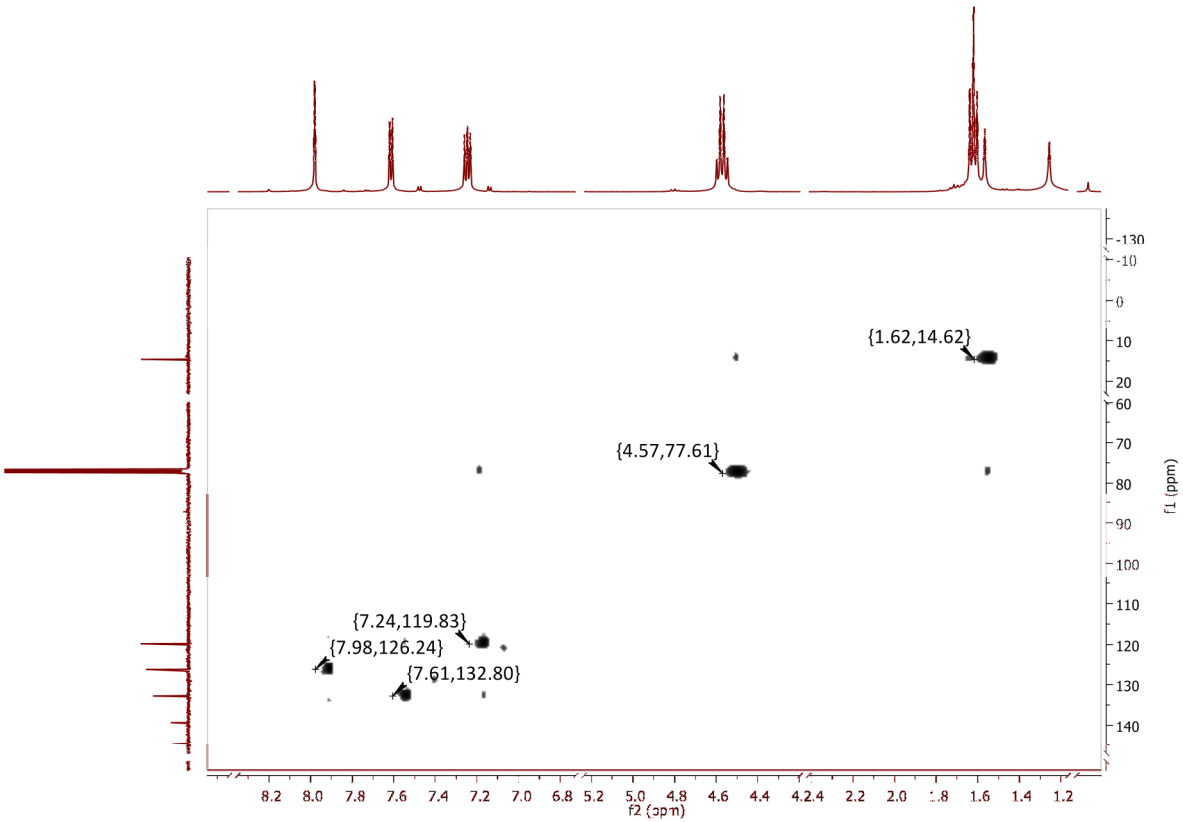

Figure S17: 2D [^{1}H, ^{13}C] HSQC NMR spectrum of **1b** in $CDCl_3$.

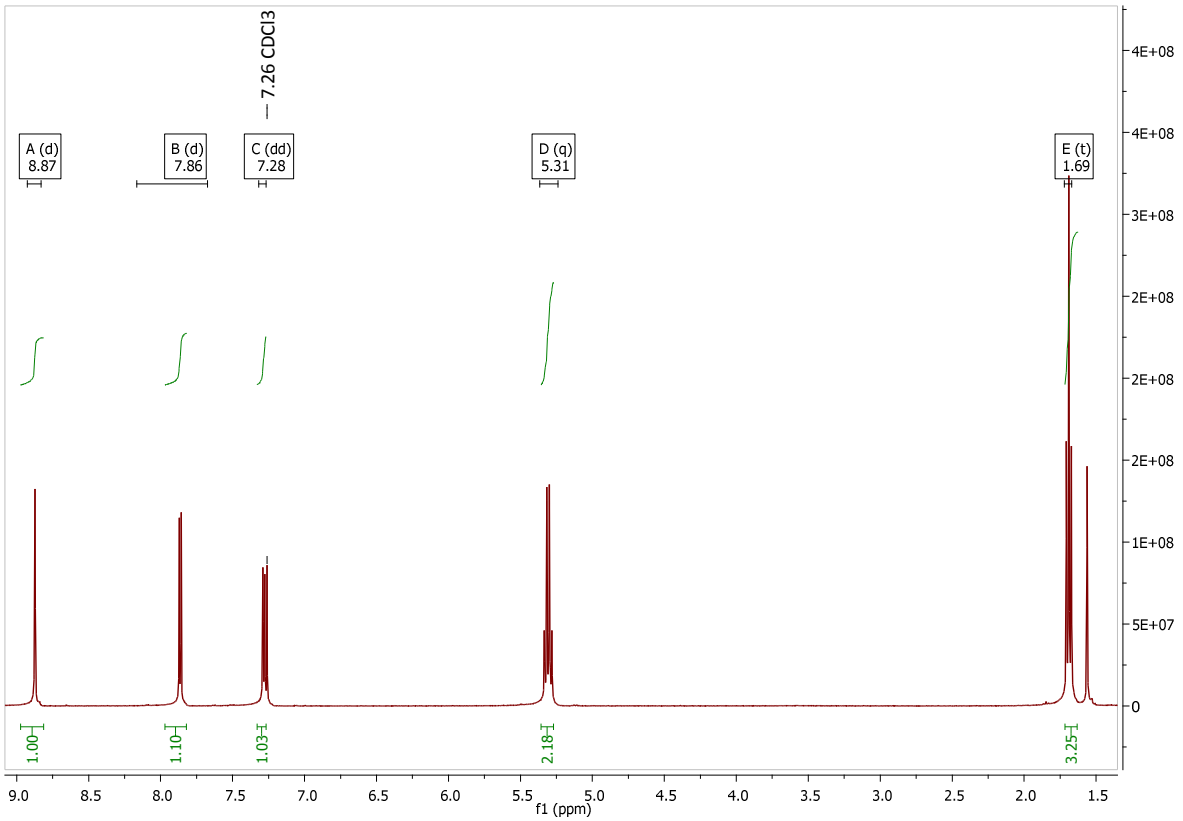

Figure S18: ^{1}H NMR spectrum of **3b** in $CDCl_3$.

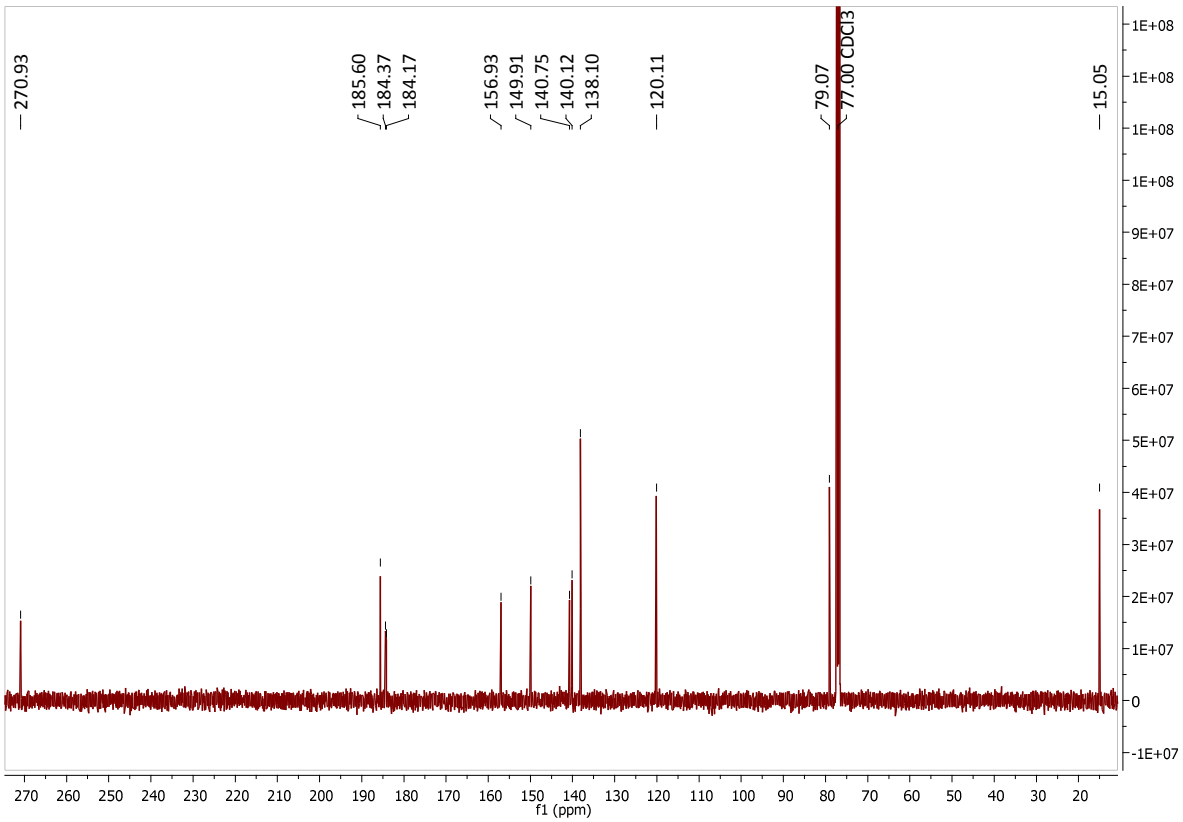

Figure S19: ^{13}C NMR spectrum of **3b** in $CDCl_3$.

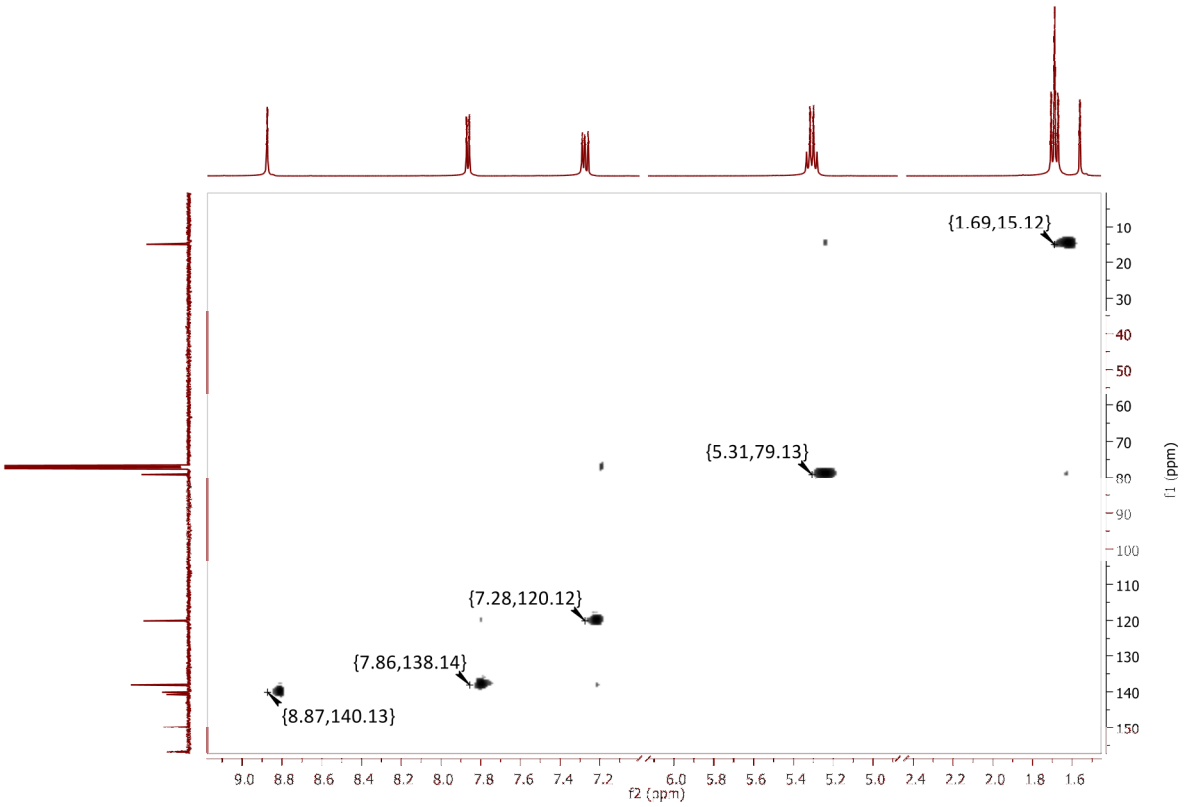

Figure S20: 2D [^{1}H, ^{13}C] HSQC NMR spectrum of **3b** in $CDCl_3$.

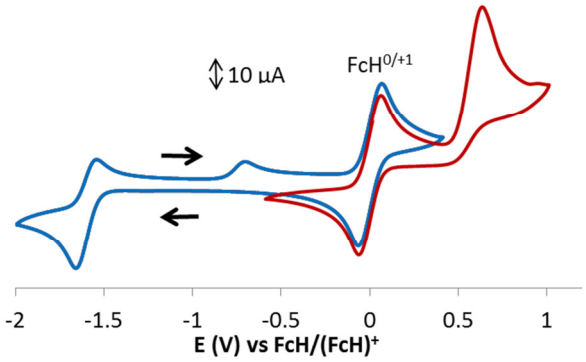

Figure S21: Cyclic voltammograms of **1a** at positive potentials (red) and negative potentials (blue), at a glassy carbon electrode, scan rate 0.1 Vs^{-1} in CH_2Cl_2 with the internal standard marked as FcH.

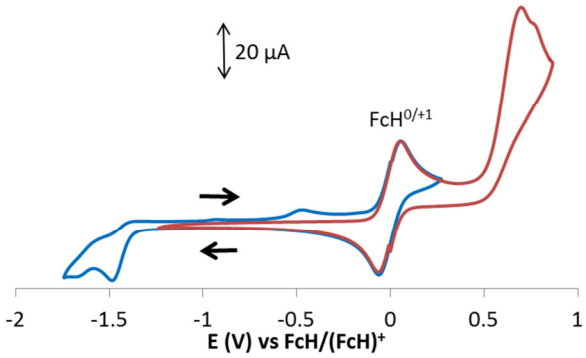

Figure S22: Cyclic voltammograms of **2a** at positive potentials (red) and negative potentials (blue), at a glassy carbon electrode, scan rate 0.1 Vs^{-1} in CH_2Cl_2 with the internal standard marked as FcH.

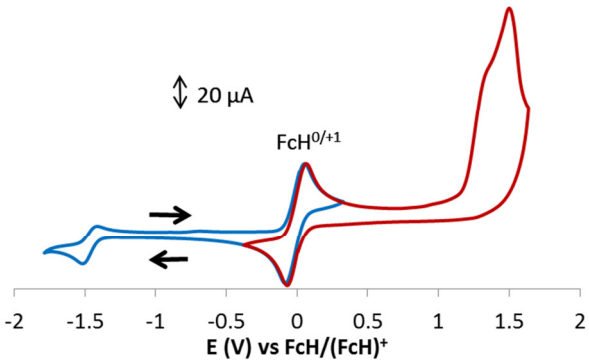

Figure S23: Cyclic voltammograms of **3a** at positive potentials (red) and negative potentials (blue), at a glassy carbon electrode, scan rate 0.1 Vs^{-1} in CH_2Cl_2 with the internal standard marked as FcH.

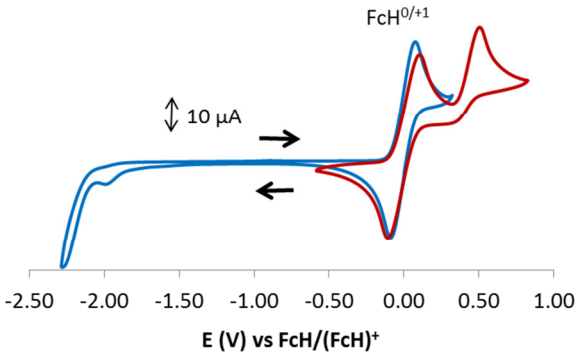

Figure S24: Cyclic voltammograms of **5a** at positive potentials (red) and negative potentials (blue), at a glassy carbon electrode, scan rate 0.1 Vs^{-1} in CH_2Cl_2 with the internal standard marked as FcH.

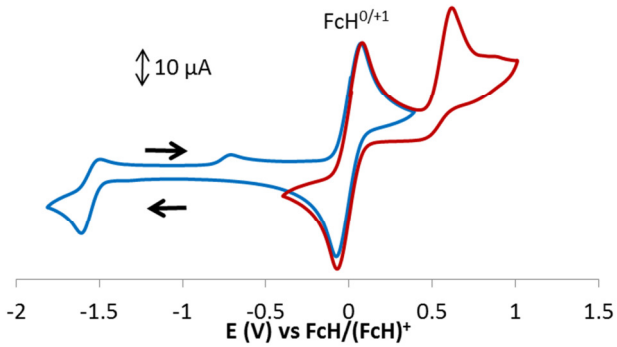

Figure S25: Cyclic voltammograms of **1b** at positive potentials (red) and negative potentials (blue), at a glassy carbon electrode, scan rate 0.1 Vs^{-1} in CH_2Cl_2 with the internal standard marked as FcH.

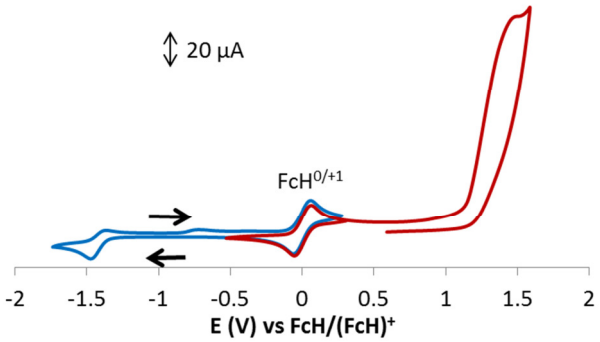

Figure S26: Cyclic voltammograms of **3b** at positive potentials (red) and negative potentials (blue), at a glassy carbon electrode, scan rate 0.1 Vs^{-1} in CH_2Cl_2 with the internal standard marked as FcH.

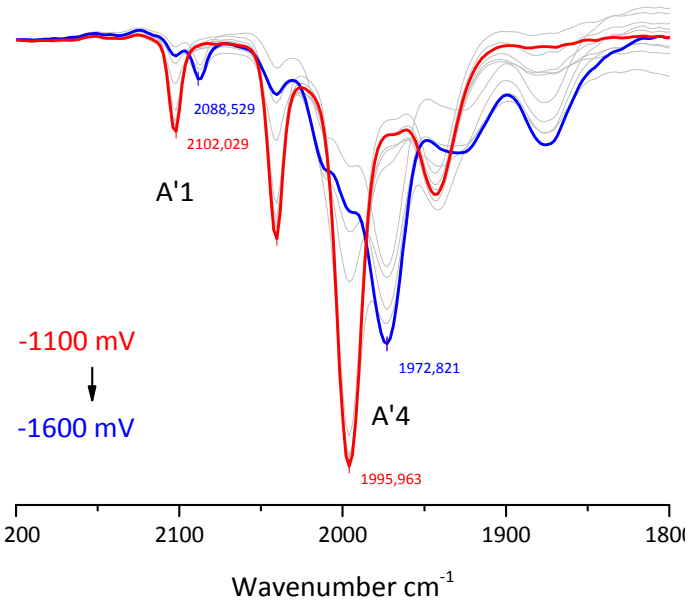

Figure S27: SEC-IR of **1a** upon reduction. Red: neutral compound; blue: reduced compound.

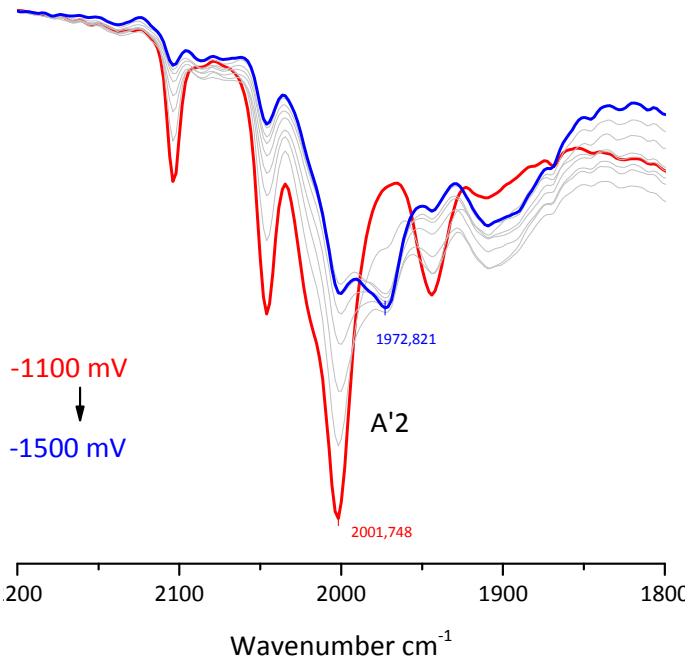

Figure S28: SEC-IR of **3a** upon reduction. Red: neutral compound; blue: reduced compound.

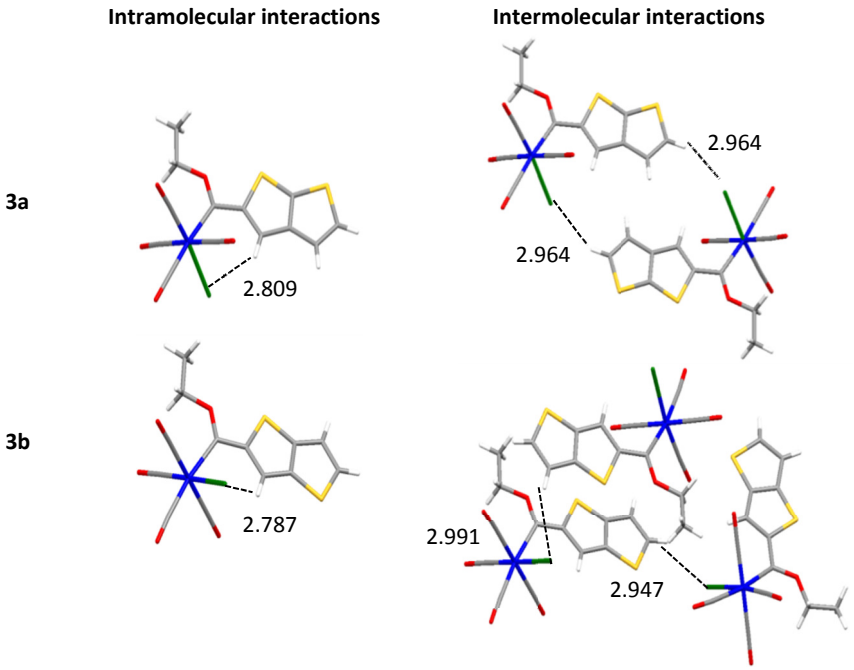

Figure S29: Intramolecular and intermolecular interactions found in the crystal packing of **3a** and **3b**.

Table S1: Crystal data and structure refinement for complexes **1a**, **2a**, **3a**, **5a**, **1b** and **3b**.

	1a	**2a**	**3a**	**5a**	**1b**	**3b**
Empirical formula	$C_{18}H_8O_{10}Re_2S_2$	$C_{30}H_{12}O_{20}Re_4S_2$	$C_{13}H_8BrO_5ReS_2$	$C_{13}H_9ClNO_4ReS_2$	$C_{18}H_8O_{10}Re_2S_2$	$C_{13}H_8BrO_5ReS_2$
Formula weight	820.76	1501.32	574.42	528.98	820.76	574.42
Temperature/K	150(2)	150(2)	150(2)	294(2)	150(2)	150(2)
Crystal system	monoclinic	monoclinic	monoclinic	monoclinic	monoclinic	orthorhombic
Space group	$P2_1/c$	$P2_1/n$	$P2_1/c$	$P2_1$	$P2_1/n$	$P2_12_12_1$
a/Å	9.6980(5)	10.1212(7)	17.2340(9)	6.5331(8)	9.6861(4)	7.3951(4)
b/Å	13.1478(6)	13.5273(11)	6.4087(4)	11.7969(16)	12.7974(5)	14.2116(10)
c/Å	17.4834(9)	14.1208(12)	16.2660(8)	10.8497(15)	17.8103(8)	15.5998(11)
α/°	90	90	90	90	90	90
β/°	106.099(2)	96.857(4)	116.6180(17)	91.742(5)	104.336(2)	90
γ/°	90	90	90	90	90	90
Volume/$Å^3$	2141.84(19)	1919.5(3)	1606.13(15)	835.80(19)	2138.96(16)	1639.48(19)
Z	4	2	4	2	4	4
$\rho_{calc}g/cm^3$	2.545	2.598	2.376	2.102	2.549	2.327
μ/mm^{-1}	11.542	12.76	10.331	7.692	11.557	10.121
F(000)	1512	1368	1072	500	1512	1072
Crystal size/mm^3	0.314 × 0.263 × 0.216	0.360 × 0.080 × 0.040	0.194 × 0.169 × 0.163	0.219 × 0.183 × 0.101	0.210 × 0.190 × 0.170	0.380 × 0.260 × 0.220
Radiation	MoKα (λ = 0.71073)	MoKα (λ = 0.71073)	MoKα (λ = 0.71073)	MoKα (λ = 0.71073)	MoKα (λ = 0.71073)	MoKα (λ = 0.71073)
2Θ range for data collection/°	4.85 to 63.298	4.696 to 54.198	5.01 to 65.296	5.102 to 54.2	4.398 to 61.014	5.222 to 56.694
Index ranges	-14 ≤ h ≤ 14, -19 ≤ k ≤ 19, -25 ≤ l ≤ 25	-12 ≤ h ≤ 12, -17 ≤ k ≤ 17, -18 ≤ l ≤ 18	-26 ≤ h ≤ 26, -9 ≤ k ≤ 9, -24 ≤ l ≤ 24	-8 ≤ h ≤ 8, -15 ≤ k ≤ 15, -13 ≤ l ≤ 13	-13 ≤ h ≤ 13, -18 ≤ k ≤ 18, -25 ≤ l ≤ 25	-9 ≤ h ≤ 9, -18 ≤ k ≤ 18, -20 ≤ l ≤ 20
Reflections collected	110751	16102	84514	17956	99281	78470
Independent reflections	7210 [R_{int} = 0.1020, R_{sigma} = 0.0438]	4222 [R_{int} = 0.0608, R_{sigma} = 0.0412]	5897 [R_{int} = 0.0828, R_{sigma} = 0.0389]	3683 [R_{int} = 0.0725, R_{sigma} = 0.0677]	6527 [R_{int} = 0.0947, R_{sigma} = 0.0368]	4087 [R_{int} = 0.0950, R_{sigma} = 0.0322]
Data/restraints/ parameters	7210/0/291	4222/0/290	5897/0/200	3683/51/224	6527/0/290	4087/12/201
Goodness-of-fit on F^2	1.061	1.061	1.06	0.94	1.066	1.178
Final R indexes [I>=2σ (I)]	R_1 = 0.0296, wR_2 = 0.0665	R_1 = 0.0303, wR_2 = 0.0563	R_1 = 0.0315, wR_2 = 0.0487	R_1 = 0.0354, wR_2 = 0.0565	R_1 = 0.0247, wR_2 = 0.0497	R_1 = 0.0269, wR_2 = 0.0612
Final R indexes [all data]	R_1 = 0.0432, wR_2 = 0.0713	R_1 = 0.0396, wR_2 = 0.0589	R_1 = 0.0468, wR_2 = 0.0520	R_1 = 0.0574, wR_2 = 0.0623	R_1 = 0.0359, wR_2 = 0.0531	R_1 = 0.0287, wR_2 = 0.0617
Largest diff. peak/hole / e $Å^{-3}$	1.64/-1.99	0.98/-1.43	1.50/-1.73	1.16/-0.61	1.21/-1.88	0.98/-2.15
Flack parameter				0.025(17)		0.406(13)
CCDC No.	1554899	1554895	1554898	1554896	1554900	1554897

Table S2: Chemical potential (μ), hardness/MO energy gap (η) and electrophilicity index (ω) reported in eV for **1a**, **1b**, **3a** and **3b**.

	1a	**1b**	**3a**	**3b**
E_{LUMO}	-3.3214235	-3.3861866	-3.3616964	-3.4561199
E_{HOMO}	-6.3603926	-6.3620253	-6.4657008	-6.4363124
μ	-4.84090805	-4.87410595	-4.9136986	-4.94621615
η	3.0389691	2.9758387	3.1040044	2.9801925
ω	7.7112962	7.983265	7.7784793	8.209219

Table S3: Major experimental UV-Vis transitions their corresponding calculated molecular orbitals for **1a**.

	Major Contributing Excitation (%)	Transition energy (nm)	Oscillator Strength	λ_{exp} (nm)	ε_{exp} ($M^{-1}cm^{-1}$)
1a	HOMO → LUMO (98)	493	0.223	450	14835
	HOMO−1→LUMO (80) HOMO →LUMO+3 (12)	393	0.219	390	12265
	HOMO→LUMO+1 (29) HOMO→LUMO+3 (49)	341	0.228	320	20995
$(1a)^-$	HOMOα→LUMO+7α (32) HOMOα→LUMO+8α (51)	538	0.0187	540	315
	HOMOα→LUMO+12α (20), HOMOβ→LUMOβ (17), HOMOβ→LUMO+3β (19)	403	0.1039	390	6100

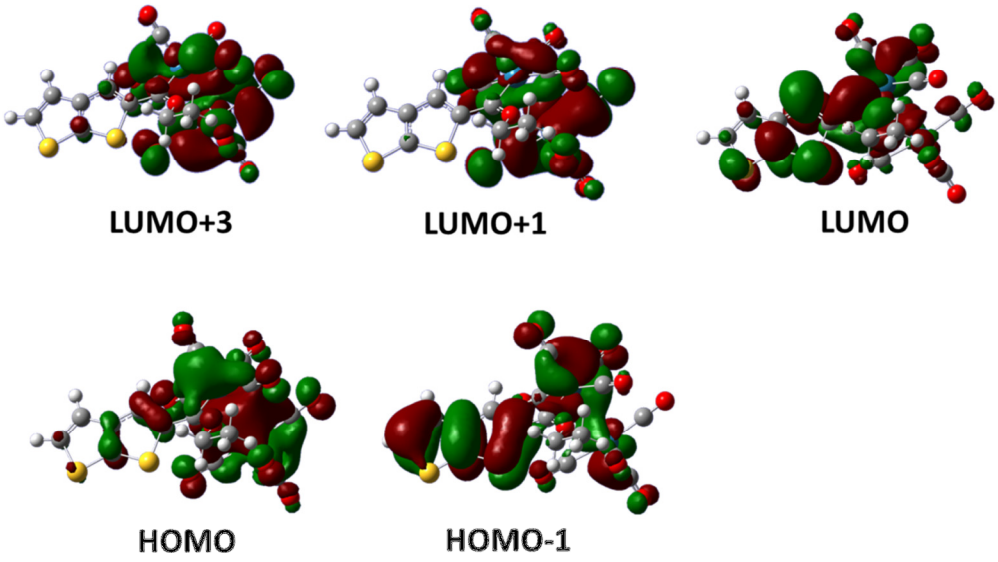

Figure S30: Normal Transition orbitals (NTOs) for the major absorption bands of **1a**.

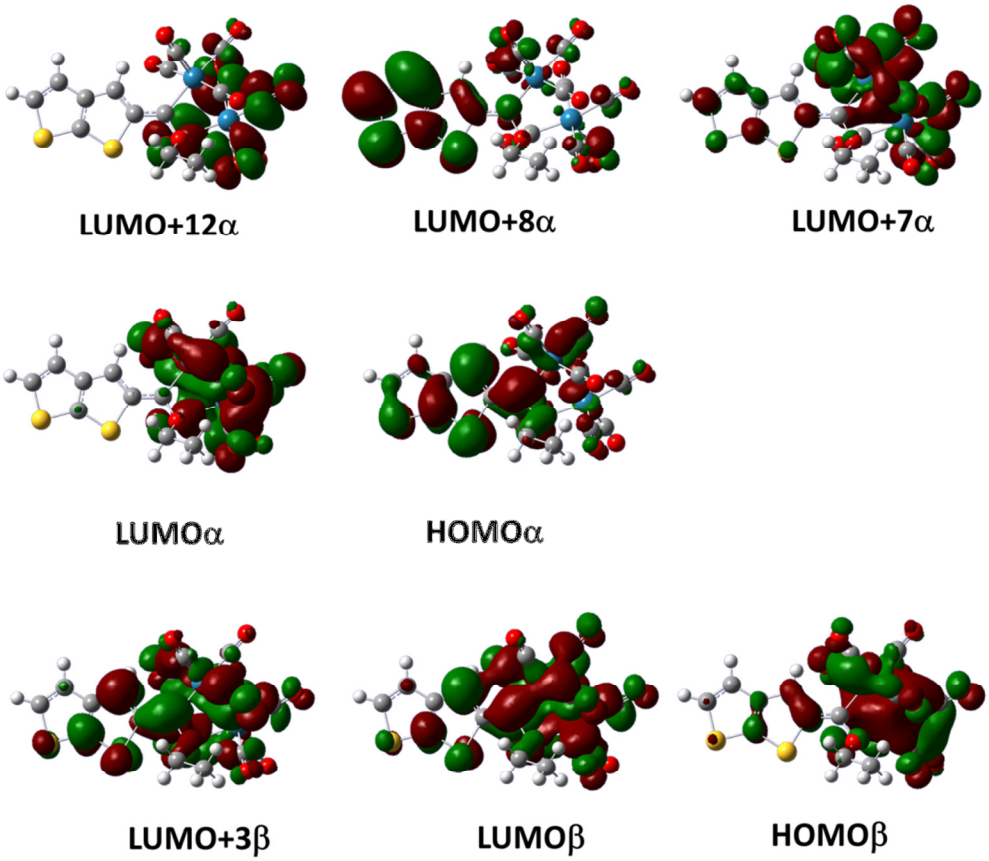

Figure S31: Normal Transition orbitals (NTOs) for the major absorption bands of **1a**$^{-}$.

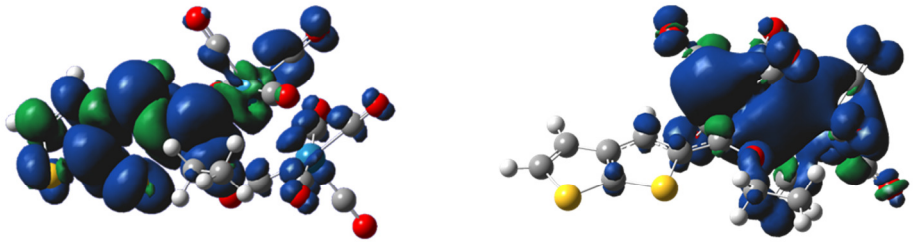

Figure S32: Spin population of **1a**$^{-}$ and **1a**$^{+}$ on the left and right hand side respectively.

Table S4: Major experimental UV-Vis transitions their corresponding calculated molecular orbitals for **1b**.

	Major Contributing Excitation (%)	Transition energy (nm)	Oscillator Strength	λ_{exp} (nm)	ε_{exp} ($M^{-1}cm^{-1}$)
1b	HOMO→LUMO (99)	497	0.2773	455	14165
	H-1→LUMO (82)	406	0.3036	395	12546
	H-5→LUMO (10) HOMO→L+1 (14) HOMO→L+3 (50)	338	0.1797	322	18907
$(1b)^-$	HOMO(A) →L+5(A) (57) HOMO(A) →L+8(A) (10) HOMO(A)->L+9(A) (10)	528	0.0126	540	391
	H-1(A) →L+1(A) (14) HOMO(A) →L+8(A) (14) HOMO(B) →LUMO(B) (19) HOMO(B) →L+2(B) (35)	434	0.1213	405	18793

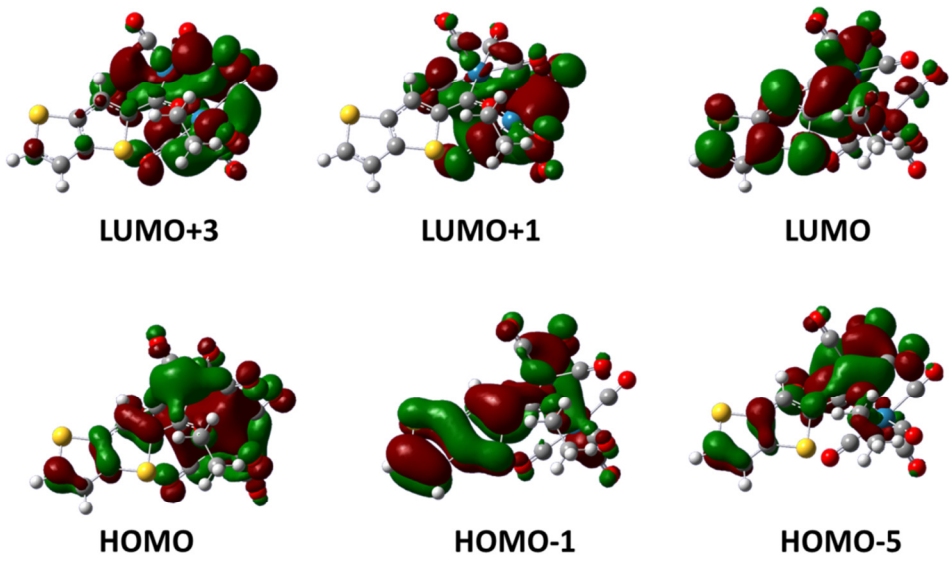

Figure S33: Normal Transition orbitals (NTOs) for the major absorption bands of **1b**.

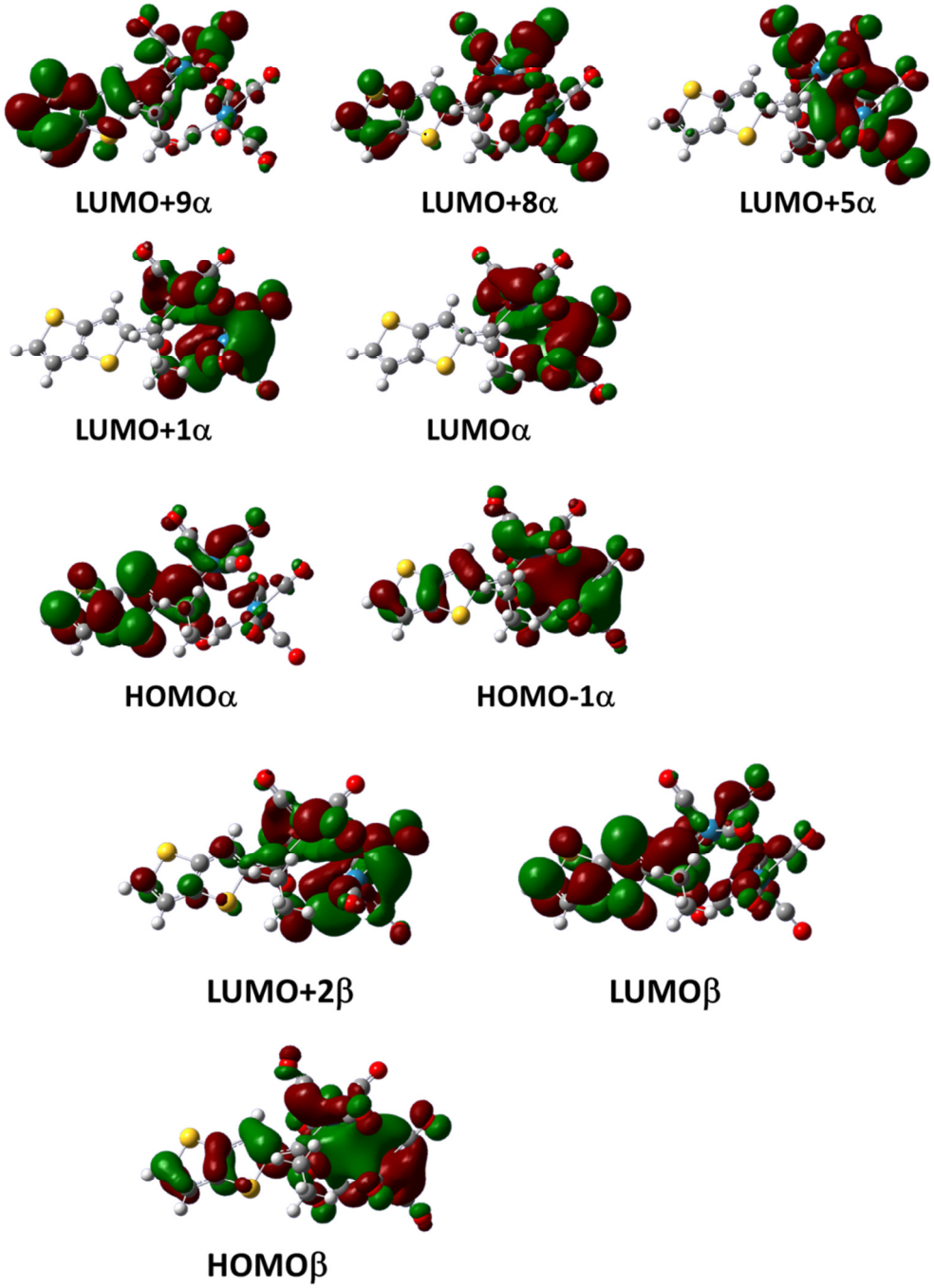

Figure S34: Normal Transition orbitals (NTOs) for the major absorption bands of **1b**$^{-}$.

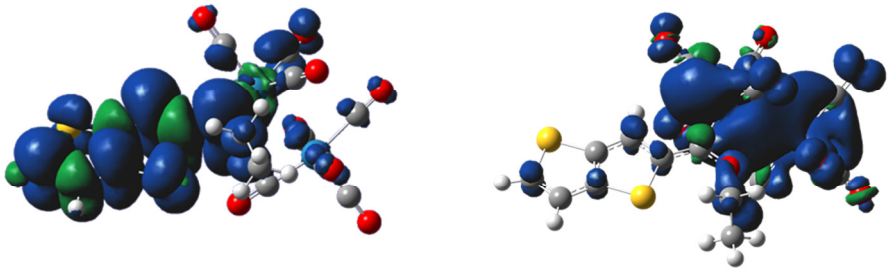

Figure S35: Spin population of **1b**$^{-}$ and **1b**$^{+}$ on the left and right hand side respectively.

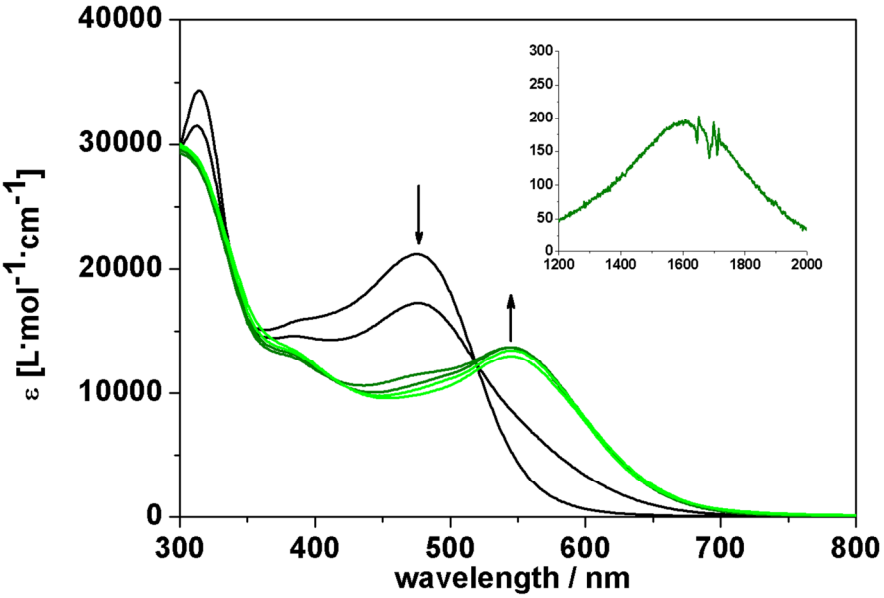

Figure S36: Changes in UV-Vis absorption spectrum of **2a** during the reduction event in CH_2Cl_2 containing 0.1 M $N^nBu_4[B(C_6F_5)_4]$ electrolyte, applied voltage range: -1.1 to -1.4 V; The inset shows the appearance of a 1600 nm Intervalence charge transfer (IVCT) feature at an applied voltage -1.4 V. (Legend: Increasing cathodic voltages from black to light green)

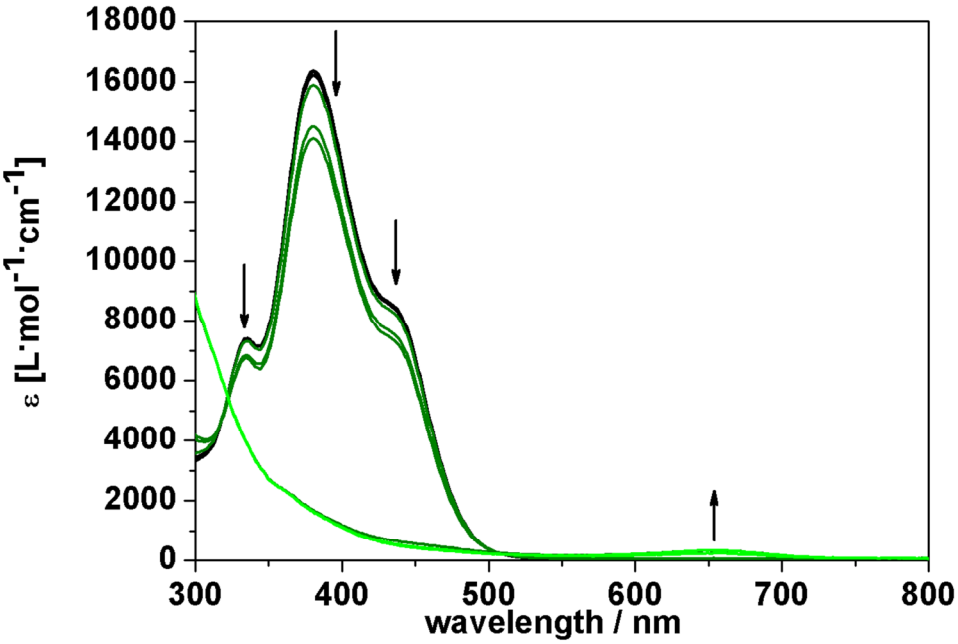

Figure S37: Changes in UV-Vis absorption spectrum of **3a** during the reduction event in CH_2Cl_2 containing 0.1 M $N^nBu_4[B(C_6F_5)_4]$ electrolyte, applied voltage range: -1.1 to -1.4 V (Legend: Increasing cathodic voltages from black to light green)

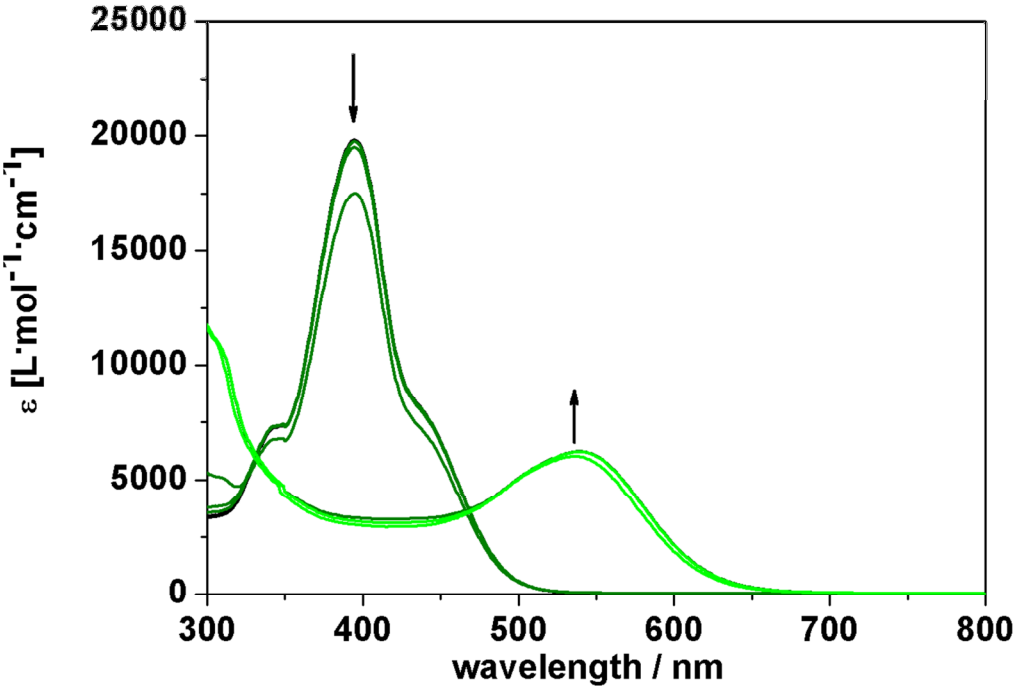

Figure S38: Changes in UV-Vis absorption spectrum of **3b** during the reduction event in CH_2Cl_2 containing 0.1 M $N^nBu_4[B(C_6F_5)_4]$ electrolyte, applied voltage range: -1.1 to -1.4 V (Legend: Increasing cathodic voltages from black to light green)